Supporting Information

The Role of Cationic Defects in Boosted Lattice Oxygen Activation during Toluene Total Oxidation over Nano-structured $CoMnO_x$ spinel

Wei Wang [a,b,c], *Yu Huang*[*a,b], *Yongfang Rao* [d], *Rong Li* [a,b,c], *Shuncheng Lee* [e], *Chuanyi Wang* [f], *Junji Cao* [a,b]

[a] State Key Laboratory of Loess and Quaternary Geology (SKLLQG), Key Laboratory of Aerosol Chemistry and Physics, Institute of Earth Environment, Chinese Academy of Sciences, Xi'an 710061, China

[b] CAS Center for Excellence in Quaternary Science and Global Change, Xi'an 710061, China

[c] University of Chinese Academy of Sciences, Beijing 100049, China

[d] Department of Environmental Science and Engineering, Xi'an Jiaotong University, Xi'an 710049, China

[e] Department of Civil and Environmental Engineering, The Hong Kong Polytechnic University, Hong Kong, China

[f] School of Environmental Science and Engineering, Shaanxi University of Science and Technology, Xi'an 710021, China

Corresponding Author and E-mail Address

*Prof. Yu Huang, E-mail: huangyu@ieecas.cn, Tel: 86-29-6233 6261

Total number of pages: 24

Total number of Schemes: 1

Total number of Figures: 9

Total number of Tables: 2

Table of contents

Catalyst Preparation. Analytically pure reagents and chemicals were used without additional purification. Typically, under vigorous stirring, $Mn(CH_3COO)_2 \cdot 4H_2O$ (2.0 mmol) and $Co(CH_3COO)_2 \cdot 4H_2O$ (1.0 mmol) were sufficiently dissolved in a well-mixed system of polyvinyl pyrrolidone (PVP, K30) (0.3 g) and ethylene glycol (EG) (38 mL) and then kept refluxing for 1 h at 170°C. Subsequently, the solution was heated to 150°C in a Teflon-lined stainless-steel autoclave and maintained for 6 h, after which the precipitate was filtrated, cleaned fully with deionized water and ethanol, and placed in a draught drying cabinet at 80°C for 12 h. Lastly, the mesoporous hollow $CoMnO_x$ microspheres were obtained by annealing the above-gained powders at 500°C for 4 h.

Catalyst characterizations. The phase structure of the sample was determined using an X-ray diffractometer with Cu Kα radiation (XRD, PANalytical X'pert). The Brunauer-Emmett-Teller (BET) surface area and pore structure were analyzed with a Gemini VII 2390 analyzer (Micromeritics Instrument ASAP 2020). The catalysts were pretreated with N_2 flow for 6 h at 150°C prior to testing. To identify the surface composition of catalysts, the survey and narrow scans on the catalyst were conducted by an X-ray photoelectron spectrometer constructed with a 150 W monochromatic Al Kα radiation (XPS, Thermo Scientific Escalab 250 Xi). As a reference, the recognized binding energy of 284.6 eV for C 1s was used. The molecular structures of the samples were obtained using a Raman spectrometer (HORIBA LabRAM HR 800) equipped with an Ar laser light of 633 nm. A classical fast-fast coincidence lifetime spectrometer (Ortec Company) was used, with a channel width of 13.0 ps and a time resolution of 220 ps, to measure the positron annihilation lifetime spectroscopy (PALS) and identify the distribution of defects. X-ray absorption fine structure spectra (XAFS) were collected using a BL14W beamline at the Shanghai Synchrotron Radiation Facility (SSRF). Electron paramagnetic resonance (EPR, Bruker ER200-SRC) was employed to detect the unpaired electrons of the samples.

The scanning electron microscope (SEM, Tescan MAIA3) and transmission electron microscope (TEM, JEOL JEM-2100F) were operated to examine the morphologies and specific details about the phase structure of the samples. Atomic-resolution spherical aberration corrected high-angle annular dark-field scanning TEM with a STEM aberration corrector (AC-HAADF-STEM, JEM-ARM200F) was used to obtain precise information on the atomic arrangement of the catalyst.

H_2 temperature programmed reduction (H_2-TPR) and O_2 temperature programmed desorption (O_2-TPD) were conducted using a chemical adsorption analyzer (BJbuilder PCA-1200) in 5% H_2/Ar and O_2 gas flow with a 5°C·min^{-1} heating rate to 900°C. Before measurement, samples (40-60 mesh) were processed at 250℃ for 1 h in He gas flow with 30 mL·min^{-1} total flow.

Operando diffuse reflectance infrared Fourier transform spectra (DRIFTS) experiments were performed in the 600-4000 cm^{-1} spectrum at 4 cm^{-1} resolutions with a scan of 32 times to detect the change of the catalyst's surface during the catalytic reaction, using a FTIR spectrometer (Bruker Vertex 70) containing a mercury-cadmium-telluride (MCT) detector. The samples were cleaned for 40 min at 230°C in a 50 mL min^{-1} N_2 flow before testing. A background spectrum was detected after pretreatment. Then, 50 ppm of toluene/N_2 was unremittingly fed into the in-situ reaction tank at 30 mL min^{-1} flow for 0.5 h at each temperature period (230°C and the following temperature of 250°C) to achieve adsorption stage equilibrium. Spectra were detected and acquired in real time. Following that, a 30 mL min^{-1} O_2/N_2 flow was continually went through the reaction tank for 0.5 h to achieve oxidation stage equilibration at 250℃, and the spectra were continually monitored.

Calculation of defect concentrations. The amounts of total metal defects (V_{tot}), manganese defects (V_{Mn}), and cobalt defects (V_{Co}) in CMO-Ex (x = 0, 0.05, 0.5) spinels are defined as the normalized ratio of deficient total metal (M), Mn, or Co atoms to the actual total number of Mn, Co, and O atoms, respectively.

$$V_{tot}\ (\%) = (0.75 - M/O) / (1 + M/O) \quad \text{(S1)}$$

$$V_{Mn}\ (\%) = (Mn/4 - Mn/O) / (1 + M/O) \quad \text{(S2)}$$

$$V_{Co}\ (\%) = (Co/4 - Co/O) / (1 + M/O) \quad \text{(S3)}$$

where 0.75 was the theoretical stoichiometric ratio of (Co, Mn)(Co, Mn)$_2$O$_4$ without cationic defects; Mn/4 and Co/4 are the Mn/O or Co/O ratios derived from the chemical formulas of stoichiometric (Co, Mn)(Co, Mn)$_2$O$_4$ without cationic defects, which can be inferred from Mn/Co and Co+Mn =3; M/O, Mn/O, and Co/O are calculated using the measured atomic ratio of Mn, Co and O by XPS.

Normalization of the DRIFTS data. The DRIFTS data were normalized using the formula as follows:

$$x^*_{i,j} = (x_{i,j} - x_j^{min})/(x_j^{max} - x_j^{min}) \quad \text{(S4)}$$

where x_j is the target infrared wavenumber (cm^{-1}), $x_{i,j}$ represents the absorbance of x_j, $x^*_{i,j}$ means the normalized peak intensity of x_j. x_j^{min} and x_j^{max} represent the minimum and maximum absorbance of the column in which x_j resides respectively.

Density functional theory (DFT) calculation details. The Vienna *ab initio* simulation package (code VASP 5.3.5),[1, 2] which uses a generalized gradient correlation functional, was used to conduct DFT calculations.[3] For Mn 3d and Co 3d, all computations were completed using the same generalized gradient approximation methods with DFT+U (U–J = 2.5 eV[2]). A plane wave cutoff of 400 eV was set, and the total energy converged to 400 eV. The Hellmann–Feynman atomic forces were minimized to less than 0.02 eV $Å^{-1}$ for all atoms. A 2 × 2 × 1 supercell of (Co, Mn)(Co, $Mn)_2O_4$ with the (1 0 0) facet exposure was first relaxed with Co atoms and Mn atoms at the upper level. The slabs of seven atomic layers separated by 11.5 Å vacuum were used to model the simulated surfaces. The calculated bond lengths are consistent with the published values.[4] The adsorption energy (E_{ads}) is defined as

$$E_{ads} = E_{tot} - (E_{sub} + E_{mol}) \quad \text{(S5)}$$

where E_{tot}, E_{sub}, and E_{mol} respectively depict the total energy of the adsorbed complex, substrate, and isolated molecule.

Scheme S1. Preparation of the porous hollow $CoMnO_x$ spinel microspheres with cationic defects.

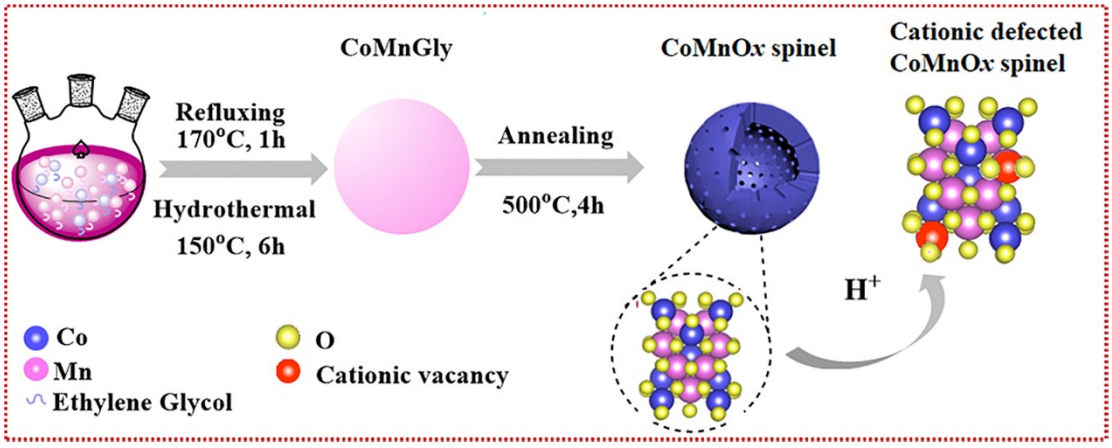

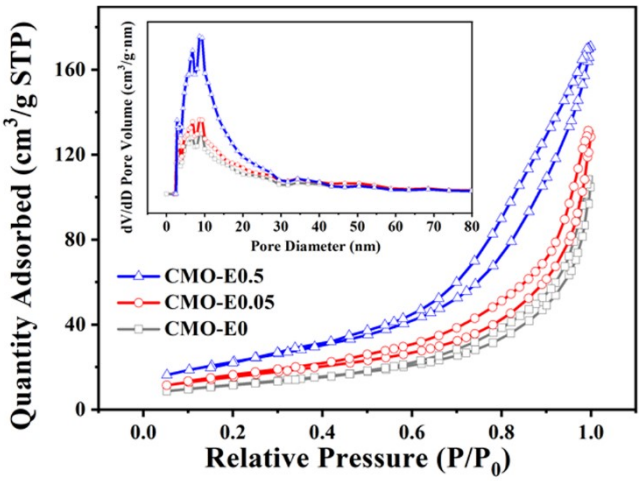

Fig. S1. N_2 adsorption-desorption isotherms of CMO-E*x* (*x* = 0, 0.05, 0.5) samples. Inset: the related BJH pore size distributions.

For all samples, an isotherm of type IV was presented with a characteristic hysteresis loop, demonstrating their mesoporous character. Generally, the mesoporous structure favors the diffusion of the reactants and the approachability of the active sites.[5] The surface area, adsorption capacity, and mean pore size of the CMO-E*x* (*x* = 0, 0.05, 0.5) samples followed in the order of CMO-E0 < CMO-E0.05 < CMO-E0.5 (Table S2), which possibly resulted from the higher numbers of mesoporous in the acid treated sample. However, according to the areal conversion rate and TOF (Table S1), the specific surface area showed no obvious influence on the instinct activity of the CMO-E*x* (*x* = 0, 0.05, 0.5).

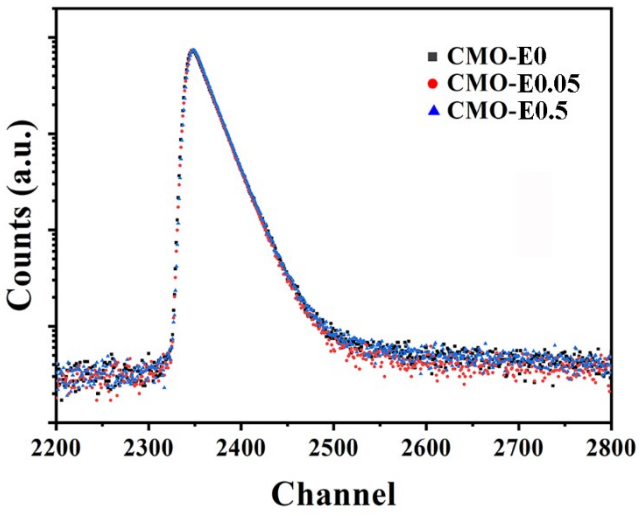

Fig. S2. Positron lifetime spectrum of CMO-Ex (x = 0, 0.05, 0.5) samples.

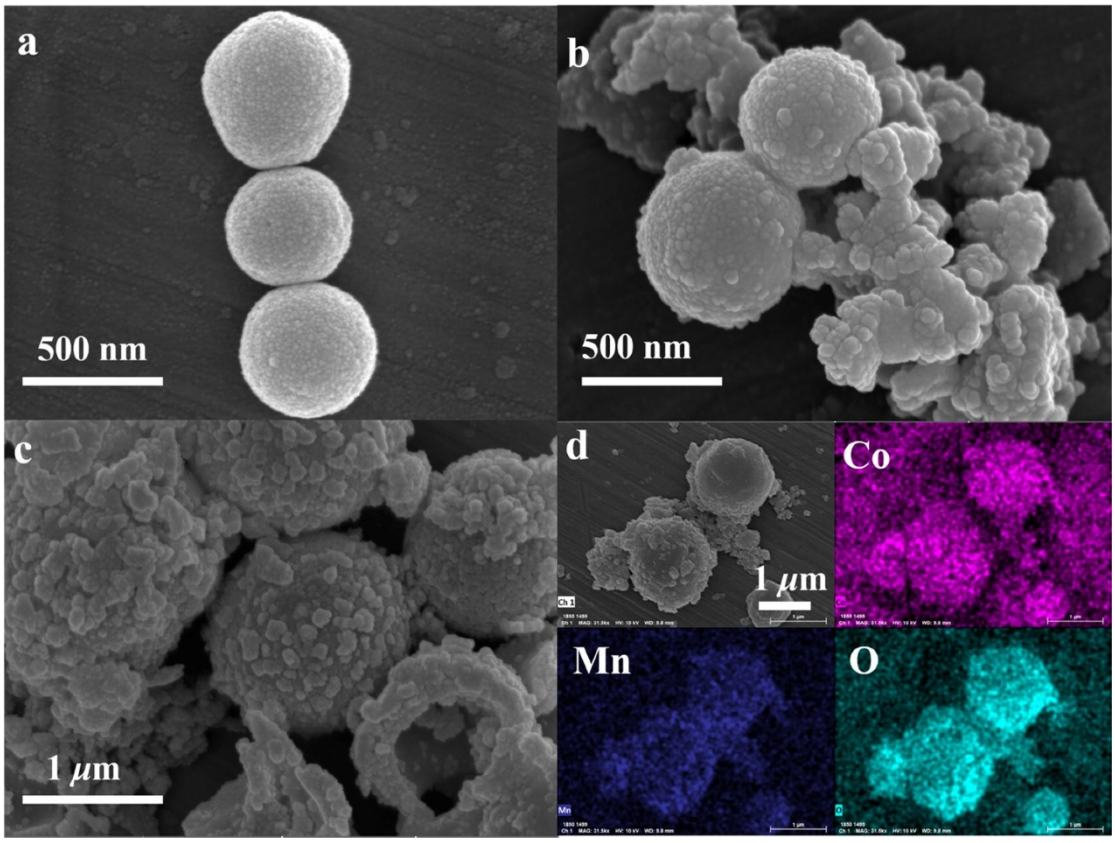

Fig. S3. SEM images of the CMO-E0 (a), CMO-E0.05 (b), and CMO-E0.5 (c); the elemental mapping images of CMO-E0.5 sample (d).

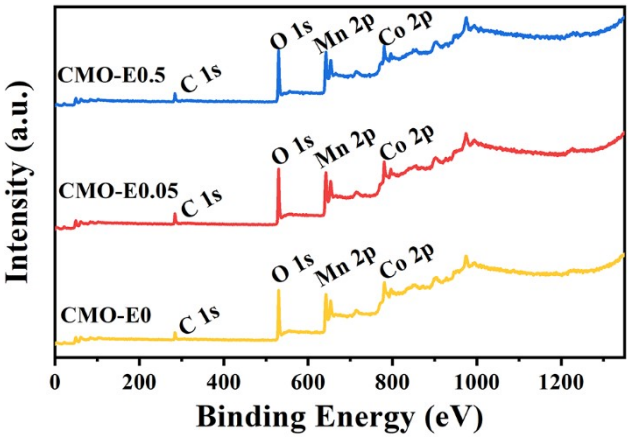

Fig. S4. XPS spectra of full survey of the CMO-E*x* (*x* = 0, 0.05, 0.5) samples.

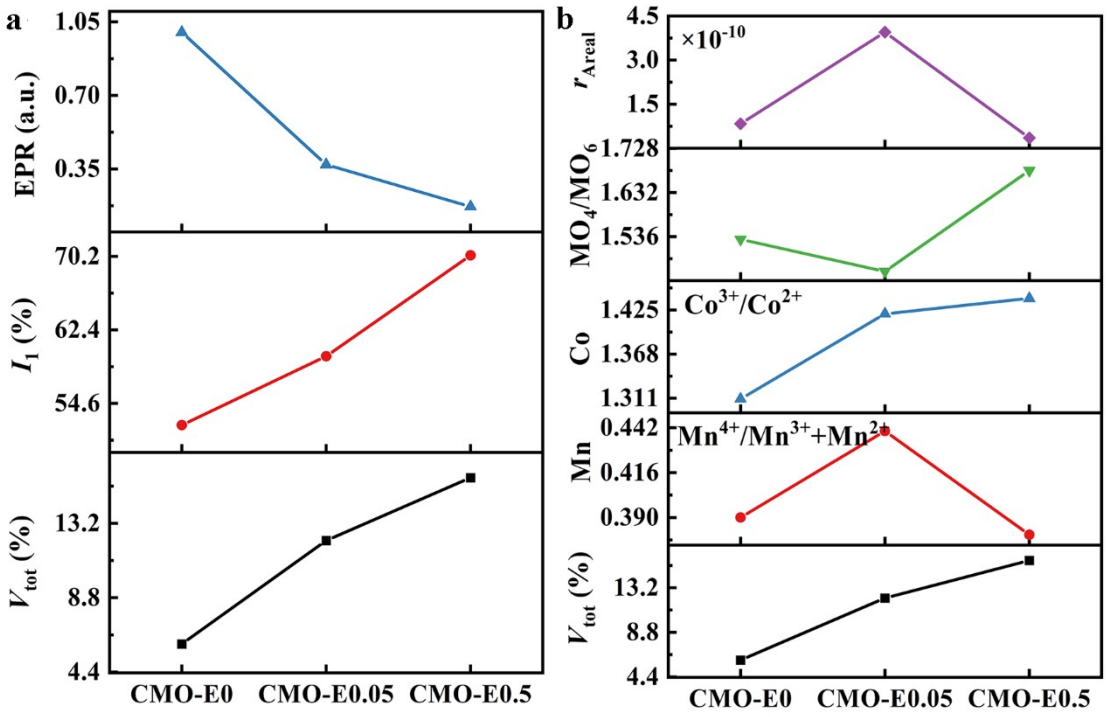

Fig. S5. CMO-Ex (x = 0, 0.05, 0.5) spinels versus the total metal defect content, relative intensities of metal defects, and EPR intensity (a), and molar ratios of $Mn^{4+}/(Mn^{3+}+Mn^{2+})$, Co^{3+}/Co^{2+}, MO_4/MO_6, and areal reaction rate at 230 °C.

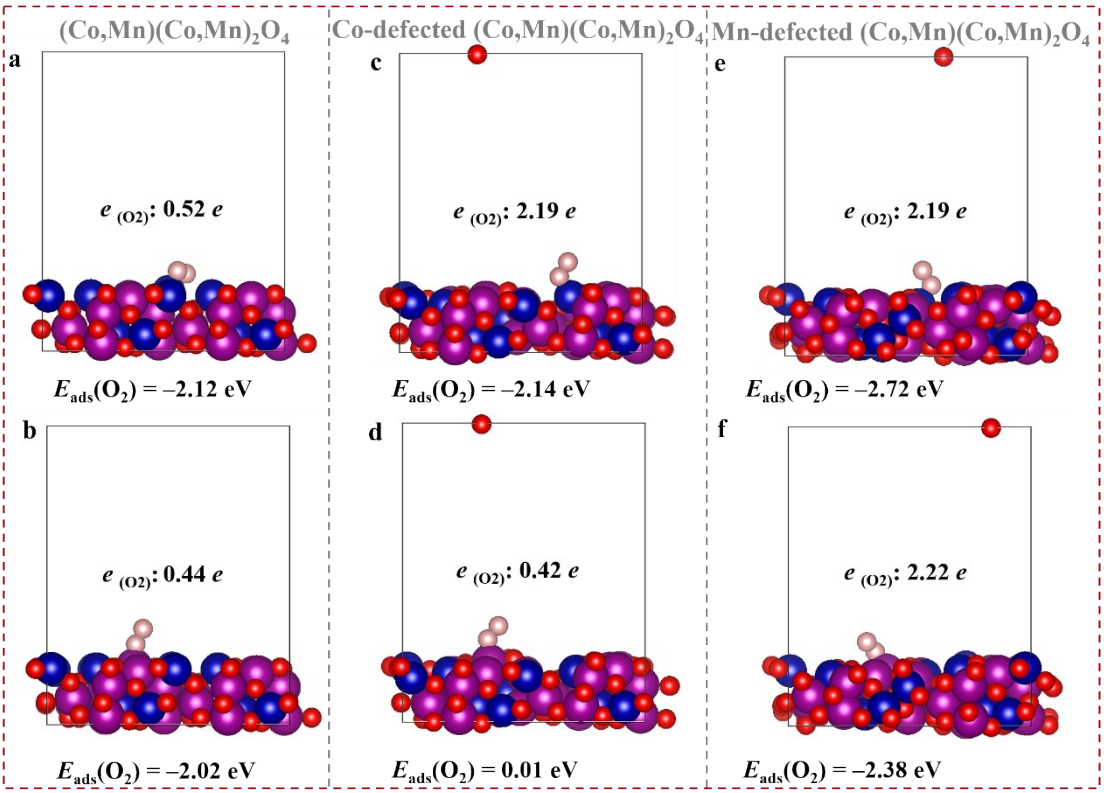

Fig. S6. Optimization of O_2 molecules (pink) on cobalt (blue) (top) and manganese (purple) (down) sites of defect-free (a-b), cobalt defect sites (c-d), and manganese defect sites (e-f) of (Co, Mn)(Co, Mn)$_2$O$_4$ surface, respectively. E_{ads} refers to the adsorption energy for O_2 molecules, and negative values mean heat release process; $e_{(O2)}$ refers to the obtained electron of O_2 molecules after adsorption.

The O_2 adsorption-activation affects the supplement of consumed lattice oxygen. To gain insight into O_2 chemisorption on the CoMnO_x spinel system surface with cation defects, DFT calculations were adopted to study the O_2 molecule adsorption configuration on defect-free cobalt and manganese sites, as well as Co defect and Mn defect sites of (Co, Mn)(Co, Mn)$_2$O$_4$, respectively, as shown in Fig. S6. The (Co, Mn)(Co, Mn)$_2$O$_4$ surface with an Mn defect showed preferable O_2 molecule binding capacity compared to that of both defect-free and Co defect surfaces from the O_2 adsorption energy. Furthermore, the electronic analysis showed that O_2

obtained more electrons from the Co-O-Mn sites on the defected (Co, Mn)(Co, Mn)$_2$O$_4$ surface than from those on the defect-free surface, indicating that cationic defects promote the activation of O_2 molecules, leading to the easy dissociation of O_2 molecules. These results demonstrate that cationic defects, especially Mn defects, can promote gaseous O_2 adsorption and activation, which is conductive to the supplement of consumed lattice oxygen, thereby boosting the intrinsic catalytic activity of $CoMnO_x$ spinels towards toluene oxidation.

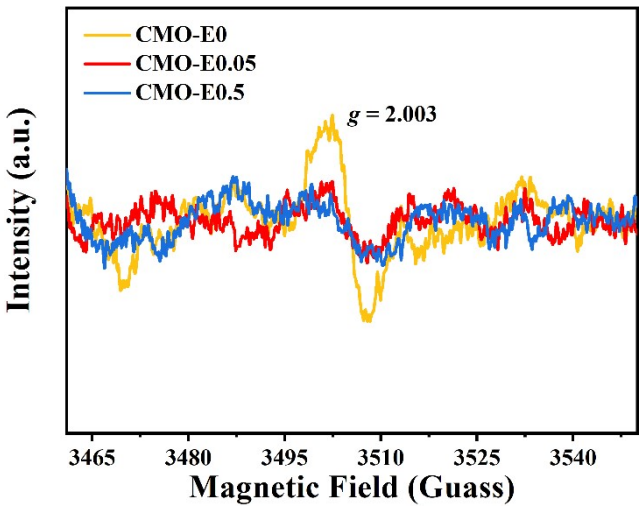

Fig. S7. EPR spin-trapping spectra of CMO-E*x* (*x* = 0, 0.05, 0.5) spinels at room temperature.

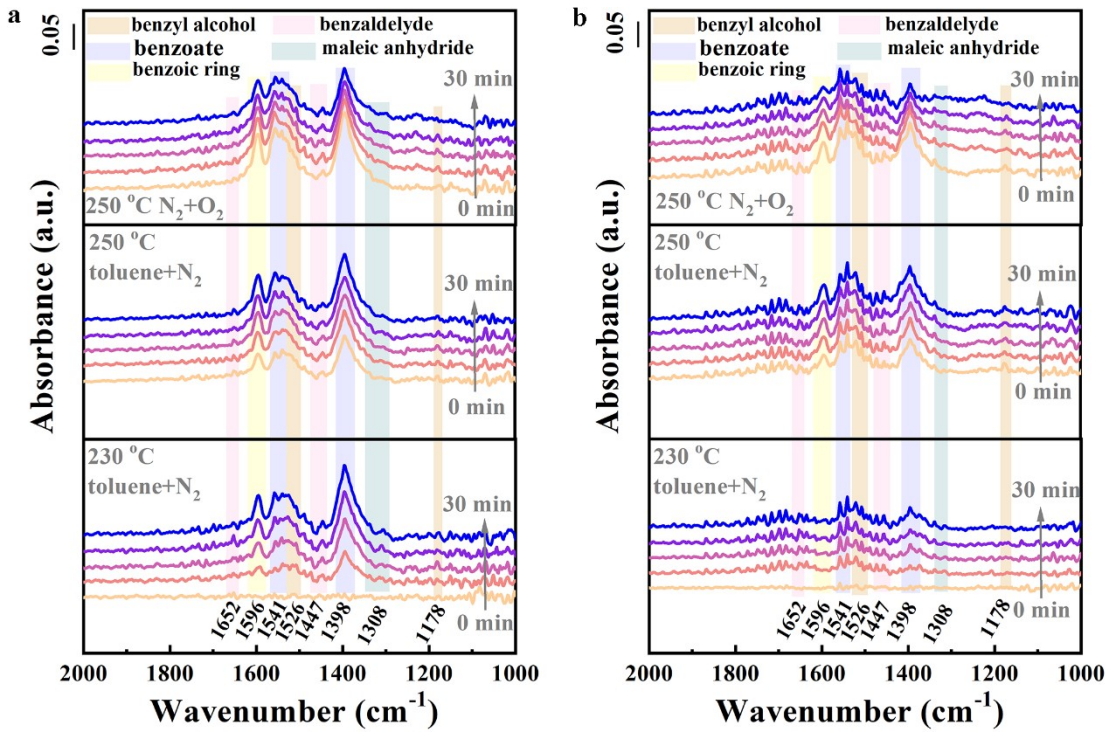

Fig. S8. Operando DRIFTS spectra of toluene adsorption and oxidation at 230~250 °C for different reaction time on CMO-E0 (a) and CMO-E0.5 (b).

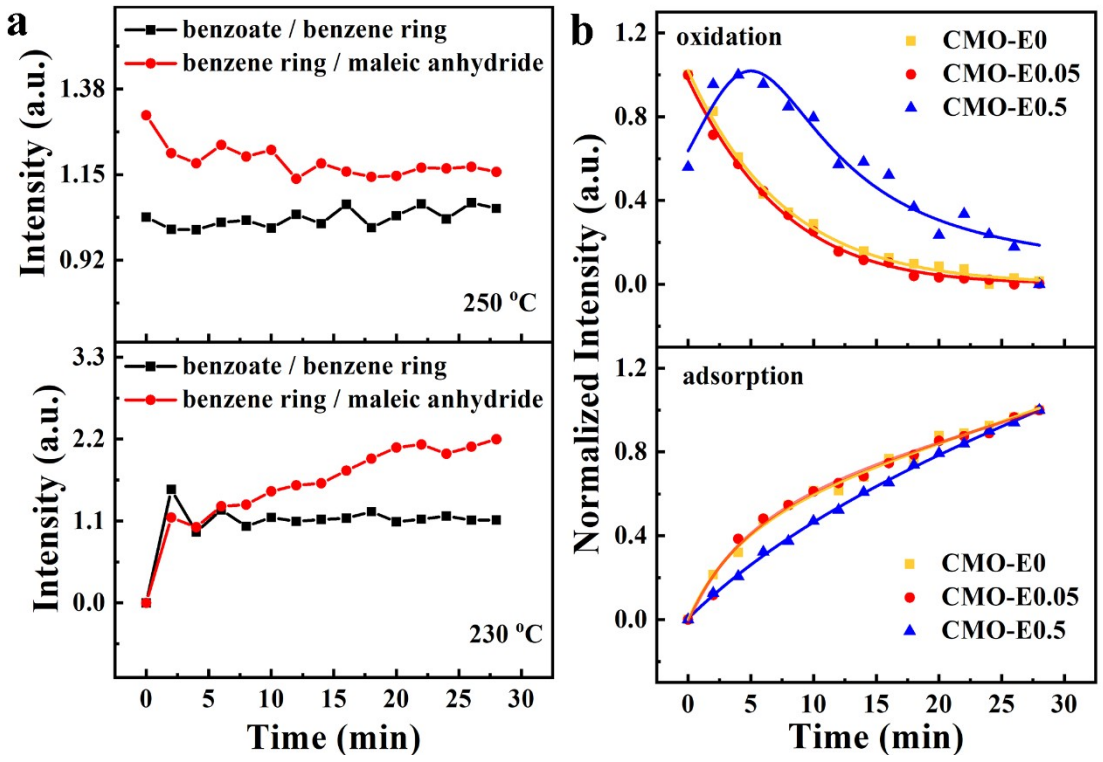

Fig. S9. (a) Time-resolved evolution curves of the intensity ratio of benzoate to active benzene and active benzene to maleic anhydride of the CMO-E0.05 during the toluene adsorption stage at different temperature. (b) Plots of accumulation and consumption of the activated benzene ring upon passing O_2+N_2 flow on CMO-E*x* (*x* = 0, 0.05, 0.5) samples after the samples pre-adsorbed toluene for 60 min.

Table S1. Catalytic properties of the CMO-E*x* (*x* = 0, 0.01, 0.05, 0.1, 0.5) samples.

Sample	Catalytic activity (°C)			r (10^{-9}·$mol_{toluene}$·g^{-1}·s^{-1}) [a]	Areal conversion Rate (r_{Areal}, μmol·m^{-2}·s^{-1})	E_a (kJ·mol^{-1})	TOF (10^{-6}·s^{-1}) [b]
	T_{10}	T_{50}	T_{90}				
CMO-E0	230	246	257	3.53	0.83×10^{-7}	177	1.00
CMO-E0.01	221	236	249	9.32	–	143	/
CMO-E0.05	206	227	238	22.1	3.95×10^{-7}	134	8.16
CMO-E0.1	228	244	256	4.43	–	157	/
CMO-E0.5	234	254	277	2.86	0.35×10^{-7}	202	1.62

[a] Reaction rate of toluene oxidation under 230 °C. Reaction conditions: 1000 ppm toluene, 21% O_2, 90 000 mL·g^{-1}·h^{-1} WHSV.

[b] TOF at 230 °C. Reaction conditions: 1000 ppm toluene, 21% O_2, 90 000 mL·g^{-1}·h^{-1} WHSV.

Table S2. Structure parameters of the cationic defected $CoMnO_x$ (CMO-E*x*, *x* = 0, 0.05, 0.5) catalysts.

Catalysts	S_{BET} ($m^2 \cdot g^{-1}$)	Pore volume ($cm^3 \cdot g^{-1}$)	Pore size (nm)	Atom ratio (%) [a]							D_{Mn} (%)[b]	M_{Td}-O/ M_{Oh}-O[c]	Co_{Td}-O/ Co_{Oh}-O[c]	Mn_{Td}-O/ Mn_{Oh}-O[c]
				Mn	Co	O	M/O	Mn/Co	$Mn^{4+}/(Mn^{3+}+Mn^{2+})$	Co^{3+}/Co^{2+}				
CMO-E0	42.6	0.15	10.19	18.48	9	42.28	0.65	2.05	0.39	1.31	35	1.53	0.55	0.98
CMO-E0.05	55.9	0.19	12.24	17.85	7.88	45.95	0.56	2.27	0.44	1.42	25	1.46	0.61	0.85
CMO-E0.5	82.3	0.25	12.40	19.19	6.26	49.90	0.51	3.07	0.38	1.44	16	1.68	0.91	0.77

[a] X-ray photoelectron spectrometry analysis. M represents Mn+Co.

[b] Mn dispersion: fraction of Mn atoms at the catalyst surface.

[c] Raman analysis. Co_{Td}-O/Co_{Oh}-O and Mn_{Td}-O/Mn_{Oh}-O represent the peak area ratio of Co_{Td}-O to Co_{Oh}-O and Mn_{Td}-O to Mn_{Oh}-O, respectively. M_{Td}-O/M_{Oh}-O presents the peak area ratio of (Mn_{Td}-O + Co_{Td}-O)/(Mn_{Oh}-O + Co_{Oh}-O).

REFERENCES

1. Kresse G, Furthmüller J. Efficiency of ab-initio total energy calculations for metals and semiconductors using a plane-wave basis set. *Comp. Mater. Sci.* 1996; **6:** 15-50.
2. Kresse G, Furthmüller J. Efficient iterative schemes for ab initio total-energy calculations using a plane-wave basis set. *Phys. Rev. B* 1996; **54:** 11169-86.
3. M E. Generalized Gradient Approximation Made Simple. *Phys. Rev. Lett.* 1996; **77:** 3865.
4. Bhatia S K, Myers A L. Optimum Conditions for Adsorptive Storage. *Langmuir* 2006; **22:** 1688-700.
5. Luo Y, Zheng Y, Zuo J *et al.* Insights into the high performance of Mn-Co oxides derived from metal-organic frameworks for total toluene oxidation. *J. Hazard. Mater.* 2018; **349:** 119-27.